




# Capillary jumps of fluid-fluid fronts across an elementary constriction in a model open fracture

Ramon Planet <sup>1,2</sup>, Lautaro Díaz-Piola <sup>1</sup> and Jordi Ortín <sup>1,2,\*</sup>

<sup>1</sup>*Departament de Física de la Matèria Condensada, Universitat de Barcelona, Martí i Franquès 1, 08028 Barcelona, Catalonia, Spain*

<sup>2</sup>*Universitat de Barcelona Institute of Complex Systems, 08028 Barcelona, Catalonia, Spain*



(Received 10 September 2019; accepted 12 March 2020; published 8 April 2020)

We study experimentally the quasistatic displacement of an oil-air front across a localized constriction in a model open fracture. The front experiences capillary jumps at one end of the constriction in both imbibition and drainage, leading to a microscale pressure-saturation hysteresis cycle. At the other end the front is reversibly pinned. A condition of local mechanical equilibrium between the restoring elasticity of the front and the distortion produced by the local change in aperture captures all we measure quantitatively, in terms of material and geometrical properties only.

DOI: [10.1103/PhysRevFluids.5.044002](https://doi.org/10.1103/PhysRevFluids.5.044002)

## I. INTRODUCTION

Two-phase flows in porous and fractured media proceed by the fluid invasion or withdrawal of individual pores and openings [1], which ultimately control the large-scale behavior of environmentally relevant processes such as secondary oil recovery, soil irrigation, and CO<sub>2</sub> sequestration [2,3]. Observations in micromodels and natural porous media using state-of-the-art imaging techniques, with optimized temporal and spatial resolution [4–12], show that local bursts at individual pores may give rise cooperatively to spatially extended, rapid fluid invasions known as Haines jumps [13]. The complexity of porous and fractured materials, however, makes the analysis of these rapid events highly challenging. Thus, even though Haines jumps are acknowledged to be the leading contribution to the energy dissipated in immiscible fluid-fluid displacements [6,14,15], their impact on imbibition-drainage hysteresis is still poorly understood and remains a subject of active research [5,16–19].

Immiscible fluid-fluid displacements through fractured and porous media are controlled at continuum scales by the relative importance of viscous to capillary forces and by the displacement direction. This leads to distinguishing *drainage* (the displacement direction in which the less wetting fluid displaces the most wetting fluid) from *imbibition* (the opposite) [1,2]. The viscosity contrast also plays a very important role: it makes the front unstable against viscous fingering when the displacing fluid is the less viscous, and stable in the opposite direction [20,21]. These two governing effects, combined, give rise to a very rich phenomenology of two-phase patterns and interfacial dynamics [22–31].

No less important, but less well understood, is the physics of local fluid motions driven by capillary forces at the scale of individual pores and throats [32–36]. Models based on capillaries of sharply varying cross section (*ink bottles*) show that fluid motion between consecutive stable interfacial configurations can be either smooth and reversible or abrupt and irreversible, depending on cross-section gradients and wettability contrast [5,13,19,37,38]. Here we extend these ideas to the motion of an oil-air interface in a Hele-Shaw cell with a localized constriction or expansion. In

---

\*jordi.ortin@ub.edu

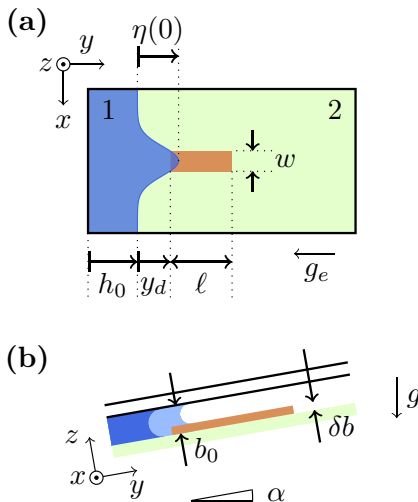


FIG. 1. (a) Top view of the Hele-Shaw cell, showing the rectangular constriction ( $w \times \ell$ ) and the distorted interface between oil (1) and air (2). Oil is injected or withdrawn from the left end (inlet), and the coordinates are  $h_0$  (distance to inlet of the flat portions of the interface),  $y_d$  (distance from  $h_0$  to the left end of the constriction), and  $\eta(0)$  (maximum height of the front with respect to  $h_0$ ). (b) Lateral view of the cell. The gap thickness is everywhere uniform,  $b_0$ , except at the localized mesa defect, where it is  $b_0 - \delta b$ . Sketches of the curved meniscus for the two different gap thicknesses are shown for zero contact angle.

contrast to the ink-bottle models, the interface here is strongly confined in one lateral dimension and spatially extended in the other. The motion in this case mimics the displacement of a two-phase fluid front in an open fracture of variable aperture. The stability of the displacement is determined by the sign of the difference  $\text{Bo} - \text{Ca}$ , where  $\text{Ca}$  and  $\text{Bo}$  are the capillary and Bond numbers, i.e., the ratio of viscous to capillary forces and of gravitational to capillary forces, respectively [39]. By tilting the cell we introduce an effective gravitational field  $g_e$  such that  $\text{Bo} > 0$ , and consider quasistatic displacements for which  $\text{Ca} \ll \text{Bo}$ . In this way we prevent viscous fingering in drainage and in imbibition. We aim at understanding the basic physics behind the motion of an extended front induced by a localized constriction or expansion. We will see that a local pressure balance at the interface accurately reproduces all the configurations observed experimentally, without having to account in detail for the complex structure of the extended meniscus. This sets the basis to later understand how localized fluid front motions give rise to large cooperative displacements (Haines jumps) in two-phase fluid displacements in disordered media.

## II. EXPERIMENTS

Our experiments were conducted in a Hele-Shaw cell consisting of two closely spaced parallel plates of size  $190 \times 500 \text{ mm}^2$  ( $x \times y$ ). The top one was a 10-mm-thick glass plate and the bottom one a fiberglass plate with a thin ( $0.060 \pm 0.010 \text{ mm}$ ) copper layer, sitting on a sturdy steel platform 15 mm thick. The plates were separated by a PVC frame which imposed controlled gap spacings  $b_0 = 0.46, 0.56, \text{ and } 0.66 \pm 0.02 \text{ mm}$ . The steel platform and the cell on top were inclined by angles  $\alpha = 2^\circ 21', 3^\circ 19', 4^\circ 9', \text{ and } 5^\circ 3' \pm 2'$ , so that an effective gravity  $g_e = g \sin \alpha$  prevented the formation of viscous fingers in drainage. *Mesa*-shaped defects were produced by carefully etching the copper layer of the fiberglass plate using standard printed circuit techniques. Constrictions were thus rectangular copper patches of thickness  $\delta b = 0.060 \pm 0.010 \text{ mm}$ , and expansions were copper-free rectangular depressions of thickness  $\delta b = -0.060 \pm 0.010 \text{ mm}$ . In either case their length was  $\ell = 60.00 \pm 0.02 \text{ mm}$  and their width  $w = 3.00, 9.00, \text{ and } 27.00 \pm 0.02 \text{ mm}$  (Fig. 1). In a complete

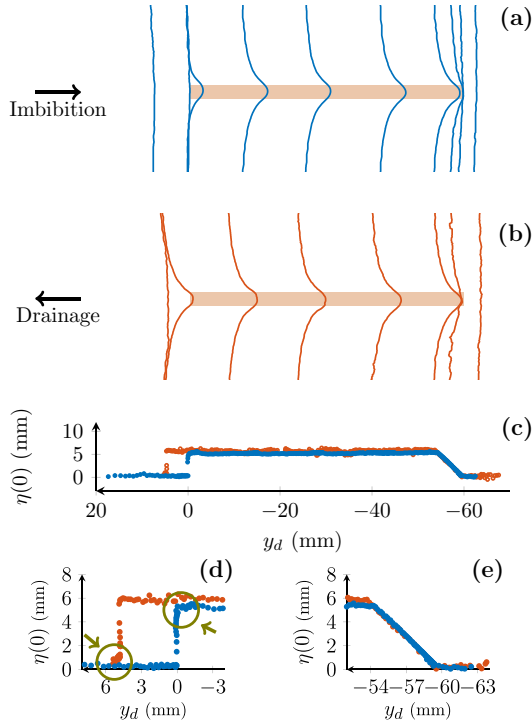


FIG. 2. Sequence of fronts recorded in oil-air displacements across a *mesa*-shaped constriction ( $\delta b > 0$ ), for imbibition (a) and drainage (b). Panel (c) shows the front deformation  $\eta(0)$  vs the relative front position  $y_d$ , in imbibition (blue dots) and drainage (red dots). Close-ups of this graph at the left and right ends of the constriction are shown in panels (d) and (e). The arrows highlight the gradual slowing down of the deformation caused by viscous dissipation at the end of each irreversible jump, as discussed in the text. Experimental parameters:  $b_0 = 0.46 \pm 0.02$  mm,  $\delta b = 0.060 \pm 0.010$  mm,  $w = 3.00 \pm 0.02$  mm,  $\ell = 60.00 \pm 0.02$  mm,  $\alpha = 4^\circ 9' \pm 2'$ .

imbibition-drainage cycle the cell was initially filled with air. A silicone oil [surface tension  $\gamma = 20.7$  mN/m, kinematic viscosity  $\nu = 50$  mm<sup>2</sup>/s, density  $\rho = 998$  kg/m<sup>3</sup>, and equilibrium contact angle with all exposed surfaces (glass, copper, and fiberglass)  $\theta \simeq 0^\circ$  at RT] was removed from or injected to the cell through its left end (inlet), and air entered or left the cell through its right end (outlet) which was open to the atmosphere. The lateral sides were sealed. Oil injection (imbibition) and withdrawal (drainage) were carried out quasistatically by changing the inlet pressure externally in very small increments and allowing the system to equilibrate after each step. Front motion was recorded with a MotionBLITZ cube6 CMOS camera with a spatial resolution of 0.24 mm/pixel. The camera was inclined by the same angle as the cell to avoid a parallax in the recorded images. Interface positions were extracted by image analysis, using classical edge detection techniques.

A sequence of front configurations recorded in an imbibition-drainage cycle across a constriction ( $\delta b > 0$ ) is shown in Fig. 2 [movie S1 of the Supplemental Material (SM) [40)]. In imbibition [panel (a)] we observed first a capillary instability right at the moment that the initially flat interface reached the left end of the constriction ( $y_d = 0$  in Fig. 1). The deformation at the centerline jumped abruptly from  $\eta(0) = 0$  to a maximum value  $\eta_c$ . The Reynolds number corresponding to the fast advancement observed in this abrupt jump was  $\text{Re} \simeq 0.4$ . Despite the large acceleration, inertial effects were negligible because of the fluid confinement and its high viscosity, as is typically the case for Hele-Shaw flows.

Following this forward jump in imbibition, the front moved with pistonlike motion and constant deformation  $\eta_c$  until the tip reached the right end of the constriction. The sequence of front

configurations that followed was strikingly different from the sequence observed at the left end. The interface progressively flattened, but the tip of the front remained pinned to the constriction until the whole front was flat, and only then did it leave the constriction.

In the reverse displacement [drainage, panel (b)] the front reached first the right end of the constriction. Its central point remained pinned there until the deformation was maximum, practically equal to the maximum deformation  $\eta_c$  reached in imbibition. This maximally deformed front then moved unchanged in a pistonlike motion across the whole constriction, until the tip reached the left end. At this stage the front depinned abruptly from the constriction and recovered its original flatness, closing the cycle.

A plot of the centerline deformation  $\eta(0)$  against the distance to the left end of the mesa defect  $y_d$  in the whole imbibition-drainage cycle [panel (c)] reveals that the two irreversible capillary events at the left end gave rise to a hysteresis cycle [panel (d)]. In contrast, front pinning at the right end was reversible, with identical deformation paths in the two directions [panel (e)]. Remarkably, analogous displacements across an expansion ( $\delta b < 0$ ) instead of a constriction displayed identical behavior with left and right ends interchanged (movie S2 of the SM [40]).

### III. THEORY

Our theoretical approach builds on the Joanny and de Gennes pioneering approach to the deformation of a contact line in the presence of wettability defects [41–43]. In the present case, however, the fluids are confined between the two close plates of a Hele-Shaw cell in one lateral dimension, so that instead of a contact line plus a free surface we have two contact lines tied together by a meniscus [44]. This changes the functional form of the propagator of the deformation, as shown below.

For a viscous fluid in a Hele-Shaw cell inertial forces are negligible, and the flow is governed by the Stokes equation. The gap-averaged, two-dimensional velocity field in each fluid satisfies Darcy’s law,

$$\vec{u}_i(x, y) = -\frac{\kappa}{\mu_i} [\nabla p_i(x, y) - \rho_i \vec{g}_e], \quad (1)$$

where  $\kappa$  is the hydraulic permeability of the cell ( $\kappa = b_0^2/12$  for uniform plate spacing  $b_0$ ),  $\mu_i$  and  $\rho_i$  are the dynamic viscosity and density of fluid  $i = 1, 2$ , and  $p_i$  is the corresponding pressure field. Ordinary liquids are incompressible,  $\nabla \cdot \vec{u}_i = 0$ , and the pressure field then obeys Laplace’s equation  $\nabla^2 p_i = 0$ . Gaseous phases have negligible viscosity,  $\mu_i \simeq 0$ , and for them the pressure field  $p_i$  is constant.

In the base state the fluid-fluid interface is flat,  $h(x, t) = h_0$ , and the two fluids move with the same velocity  $\vec{u}_i^0 = V_\infty \hat{j}$ . Taking the pressure origin at the interface ( $y = h_0 = V_\infty t$ ) the pressure distribution takes the form

$$p_i^0 = -\left(\rho_i g_e + \frac{\mu_i V_\infty}{\kappa}\right)(y - V_\infty t), \quad (2)$$

where  $g_e$  is the magnitude of the effective gravitational acceleration. If the interface is now slightly distorted from flatness (Fig. 1) such that  $h(x, t) = V_\infty t + \eta(x)$ , pressure field and velocity field are modified correspondingly:

$$p_i = p_i^0 + p_i^d \quad \text{and} \quad \vec{u}_i = \vec{u}_i^0 + \vec{u}_i^d. \quad (3)$$

Darcy’s law and the condition of fluid incompressibility apply also to these perturbed fields. The local pressure jump across a curved interface is given by the Young-Laplace equation

$$[[p]] = \gamma(\kappa_\parallel + \kappa_\perp), \quad (4)$$

where  $\gamma$  is the interfacial tension between the two fluids and  $\kappa_\parallel, \kappa_\perp$  are in-plane and perpendicular curvatures of the meniscus, respectively. The strongest curvature of the meniscus in a Hele-Shaw cell is  $\kappa_\perp$ , but in a cell of uniform gap spacing,  $b_0$ , and for a constant (static) contact angle,  $\theta$ , it can be approximated by the constant value  $2 \cos \theta / b_0$ . This approximation disregards the eventuality

that the more wetting fluid may leave coating films on the cell plates when it is displaced [45]. Since we assume that  $|\partial\eta/\partial x| \ll 1$ , we can approximate the in-plane curvature by  $\kappa_{\parallel} \simeq \partial^2\eta/\partial x^2$  to first order in  $\eta$ . The extra pressure jump across the distorted interface due to the perturbation of the front shape is thus given by

$$\llbracket p^d(x) \rrbracket \equiv p_1^d(x) - p_2^d(x) \simeq \gamma \frac{\partial^2\eta(x)}{\partial x^2} - \frac{\mu_1 - \mu_2}{\kappa} V_{\infty} \eta(x) - (\rho_1 - \rho_2) g_e \eta(x) \quad (5)$$

to linear order in  $\eta$ . The terms on the right-hand side of the equation account, respectively, for the capillary, viscous, and hydrostatic pressure contributions to the difference in pressure jump.

The difference  $\llbracket p^d(x) \rrbracket$  may be restoring or destabilizing. When  $V_{\infty} < -\kappa \Delta\rho g_e / \Delta\mu$ , where  $\Delta\rho \equiv \rho_1 - \rho_2$  and  $\Delta\mu \equiv \mu_1 - \mu_2$ , i.e., when  $\text{Bo} - \text{Ca} < 0$ ,  $\llbracket p^d(x) \rrbracket$  is destabilizing: it leads to the formation of incipient Saffman-Taylor fingers [20,21]. Very quickly, however, the linear approximation fails in this unstable case. Contrarily, for  $V_{\infty} > -\kappa \Delta\rho g_e / \Delta\mu$ , i.e.,  $\text{Bo} - \text{Ca} > 0$ ,  $\llbracket p^d(x) \rrbracket$  is restoring: it tends to bring the interface back to the flat configuration  $\eta(x) = 0$ . In this case the interface between two immiscible fluids in a Hele-Shaw cell of constant gap thickness can be regarded as an *elastic* line, which opposes a local deformation  $\eta$  with a *Hookean* elastic force  $k\eta$  (Fig. 1). The elastic response originates from the combined action of interfacial tension, viscous damping, and effective gravity.

In order to determine the spring constant associated with the “elastic” restoring force of the interface in the stable case,  $\text{Bo} - \text{Ca} > 0$ , we write Eq. (5) as  $\llbracket p^d(x) \rrbracket \simeq -\mathcal{L}\eta(x)$ , where  $\mathcal{L}$  is a linear differential operator. When a local perturbation corresponding to a pressure field  $p_a(x, y)$  produces an in-plane distortion of the interface  $y = h(x)$ , the corresponding equilibrium condition reads

$$p_a[x, h(x)] - \mathcal{L}\eta(x) = 0. \quad (6)$$

Since  $\mathcal{L}$  is a linear differential operator,

$$\eta(x) = \int_{\mathcal{R}} dx' G(x - x') p_a[x', h(x')], \quad (7)$$

where  $G(x)$  is the propagator of the elastic response of the interface to a localized disturbance. The explicit form of the propagator is obtained by solving  $\mathcal{L}G(x) = \delta(x)$ , where  $\delta(x)$  is Dirac’s delta function. In our case this equation reads

$$[\gamma q^2 + (\Delta\mu/\kappa)V_{\infty} + \Delta\rho g_e] \hat{G}(q) = 1, \quad (8)$$

in Fourier space, where  $q$  is the conjugate variable of  $x$  and  $\hat{G}(q)$  is the Green’s function in Fourier space. The result of inverting this equation depends on the sign of  $\ell_g^2 \equiv \kappa\gamma / (\Delta\mu V_{\infty} + \kappa \Delta\rho g_e)$ . Here  $\ell_g^2$  is the (squared) lateral length scale in which capillary forces prevail. For unstable fluid displacements ( $\ell_g^2 < 0$ , i.e.,  $\text{Bo} - \text{Ca} < 0$ ) the propagator in real space takes the form

$$G(x) = -\frac{\ell_g}{2\gamma} \sin \frac{|x|}{\ell_g}. \quad (9)$$

For marginally stable ones ( $\ell_g^2 = \infty$ , i.e.,  $\text{Bo} - \text{Ca} = 0$ ) it takes the form

$$G(x) = -\frac{|x|}{2\gamma}. \quad (10)$$

Finally, for stable displacements ( $\ell_g^2 > 0$ , i.e.,  $\text{Bo} - \text{Ca} > 0$ , the case of interest here) it reads

$$G(x) = \frac{\ell_g}{2\gamma} e^{-|x|/\ell_g}. \quad (11)$$

This novel propagator describes the linear “elasticity” of the interface between two immiscible fluids in a Hele-Shaw cell. Remarkably it is qualitatively different from the propagators of the restoring force of a contact line [41] or a fracture front [46,47], which depend logarithmically on

the reciprocal of the distance. We write the distorting pressure in the form  $p_a[x, h(x)] = p_a f(x)$ , where  $p_a$  is the strength of the defect and  $f(x)$  a dimensionless function  $0 \leq f(x) \leq 1$ , symmetric around  $x = 0$ . Then a Hookean (linear) relation  $p_a = k\eta(0)$  holds, where  $k = 1/\int dx' G(x')f(x')$  is the corresponding spring constant. For a mesa defect of width  $w$  the spring constant reads

$$k = \frac{\gamma/\ell_g^2}{1 - e^{-w/2\ell_g}}. \quad (12)$$

In the particular case  $\text{Ca} \rightarrow 0$ , i.e., for quasistatic displacements, the term of viscous pressure damping in Eq. (5) vanishes. In this limit the elastic response of the interface is provided only by surface tension and gravity.

In our experiment the distorting pressure is produced by a constriction (expansion), which locally reduces (increases) by  $\delta b$  the gap thickness of the Hele-Shaw cell. As a result, the curvature of the fluid-fluid meniscus across the gap of the cell changes abruptly from  $2 \cos \theta/b_0$  to  $2 \cos \theta/(b_0 - \delta b)$  on the defect (Fig. 1). In quasistatic conditions  $\theta$  can be assumed to take its static (equilibrium) value. This abrupt change in curvature produces a distorting pressure

$$p_a(x, y) \simeq 2\gamma \cos \theta \frac{\delta b(x, y)}{b_0^2} \quad \text{at } y = h(x), \quad (13)$$

which is responsible for pulling the wetting phase towards the defect when  $\delta b > 0$  (constriction) and for pushing it away when  $\delta b < 0$  (expansion). The local change in gap thickness changes locally also the hydraulic permeability of the cell (which in turn would change the viscous pressure drop in the oil phase), but these changes are irrelevant for quasistatic displacements. Similarly, the condition of continuity is always satisfied in quasistatic displacements.

From the Hookean relation  $p_a = k\eta(0)$ , the stationary deformation experienced by the front reads

$$\eta_c = 2(1 - e^{-w/2\ell_g}) \cos \theta \delta b \left( \frac{\ell_g}{b_0} \right)^2. \quad (14)$$

Figure 3 shows that this prediction is in excellent agreement with our experimental results; we emphasize that no fitting parameters are used in this comparison.

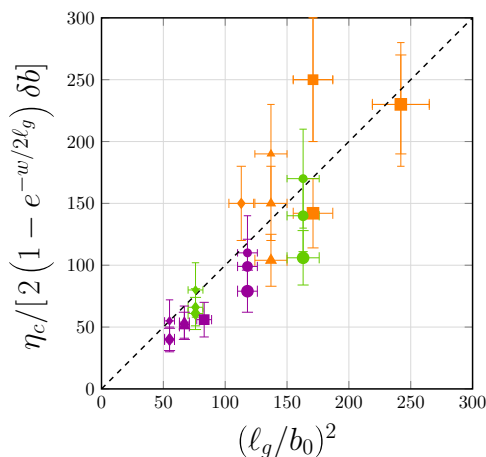


FIG. 3. Data collapse of maximum front deformations. Symbols correspond to drainage experiments with  $\delta b = 0.060$  mm,  $b_0 = 0.46$ ,  $0.56$ , and  $0.66$  mm (orange, green, and purple),  $\alpha = 2^\circ 21'$ ,  $3^\circ 19'$ ,  $4^\circ 9'$ , and  $5^\circ 3'$  (circles, squares, up-pointing triangles, and down-pointing triangles), and  $w = 3$ ,  $9$ , and  $27$  mm (small, medium, and large symbol sizes). The values of  $\eta_c$  have been obtained from averages over more than 100 images recorded in the same experiment. The dashed line is the theoretical prediction of Eq. (14) for  $\theta = 0^\circ$ .

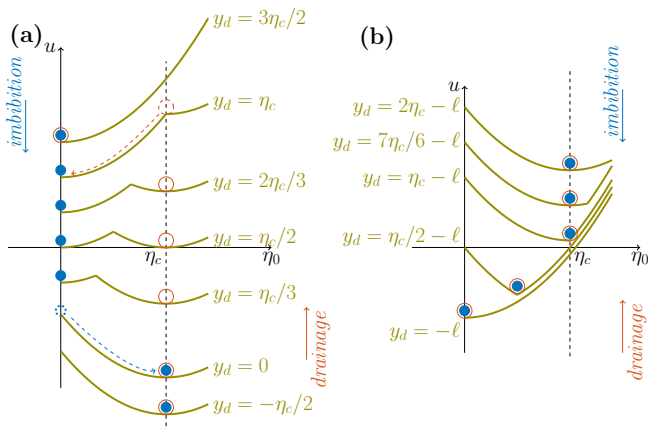


FIG. 4. Qualitative behavior of the energy density function of the two-fluid system in the presence of a positive mesa defect ( $p_a > 0$ ) as a function of the centerline front deformation  $\eta_0$ . In both panels the system follows the downward sequence in imbibition and the upward sequence in drainage; the vertical dashed line shows the maximum front deformation,  $\eta_c$ ; and the equilibrium configurations are shown as solid blue dots in imbibition and open red dots in drainage. (a) Left end of the defect. (b) Right end of the defect.

Further physical insight can be gained from energy considerations [41]. Firstly, the fluid front behaves as an elastic spring whose elastic energy density is  $u_{el} = k\eta_0^2/2$ , where  $\eta_0 \equiv \eta(0)$ . Secondly, the work done by the localized expansion or constriction in deforming the front is  $u_W = -p_a(\eta_0 - y_d)$ . The energy density of the fluid-fluid interface can then be built as a piecewise function of its distance to the mesa defect,  $y_d$ , which is controlled externally by the applied pressure:

$$u(\eta_0, y_d) = \begin{cases} \frac{1}{2}k\eta_0^2, & \eta_0 < y_d \\ \frac{1}{2}k\eta_0^2 - p_a(\eta_0 - y_d), & y_d < \eta_0 < y_d + \ell \\ \frac{1}{2}k\eta_0^2 - p_a\ell, & \eta_0 > y_d + \ell. \end{cases} \quad (15)$$

The shape of  $u(\eta_0, y_d)$  for a constriction ( $\delta b > 0$ ) is shown in Fig. 4 for different values of  $y_d$ . In panel (a) we see that the two irreversible capillary events at the left end of the constriction, in the absence of external fluctuations, arise from the disappearance of the energy barrier separating the equilibrium states  $\eta_0 = 0$  and  $\eta_c = p_a/k$ . These two nonequilibrium jumps involved in the drainage-imbibition hysteresis cycle of Fig. 2 give rise therefore to large and abrupt dissipations of elastic energy. Indeed, the corresponding elastic waves have been measured as acoustic emissions in the passage of fluid fronts within assemblies of glass beads [48]. Panel (b), in contrast, shows the reason why the front pinning observed at the right end of the constriction is reversible: the stable minima at pinning are located now at the crossing points of the last two pieces of Eq. (15), which are the same in imbibition and drainage, and correspond to smoothly varying deformations of the front. An equivalent analysis in terms of pressures instead of energies is provided in the SM [40].

#### IV. DISCUSSION AND CONCLUSIONS

We have studied the interfacial dynamics of two-phase fluid displacements across a localized constriction or expansion in a Hele-Shaw cell. Our results highlight the rich phenomenology of the motion of interfaces over defects. Specifically, our problem lies between the ink bottle, where a completely confined interface moves through a tube of variable cross section, and the contact line, where a completely unconfined interface moves over a solid surface. In the present case the interface is extended in one lateral dimension and confined in the other, mimicking the passage of a fluid front



through an open fracture with a localized change in aperture. For stable displacements ( $Bo - Ca > 0$ ), the lateral extension of the front in one dimension has the advantage that a differential equation—the linearized Saffman-Taylor equation of motion in a Hele-Shaw cell—governs the dynamics, in contrast with the ink-bottle problem. The confinement of the interface between the two plates of the cell—quantified by the local out-of-plane curvature of the meniscus—introduces, on the other hand, the nonlinearities responsible for the variety of equilibrium and nonequilibrium behaviors observed experimentally, even in the quasistatic limit.

Our approach identifies the consecutive equilibrium states of the fluid-fluid front and their relative stability. This reveals already the hysteretic nature of imbibition-drainage cycles at the scale of individual heterogeneities. However, as the pressure balance on which it is based is valid only in quasistatic conditions, the present approach cannot account for the front dynamics during abrupt changes of  $\eta(x)$ . Not surprisingly, viscous effects become very important in those jumps, as shown by the arrows in Fig. 2(d). Departure from the quasistatic limit to account for finite flow rates leads to new research avenues that will be pursued in the future.

The model predicts also that the front should adopt the same stationary deformation,  $\eta_c$ , in both imbibition and drainage. We observe, however, in Figs. 2(d) and 2(e), a small but systematic difference. We attribute the larger deformation in drainage to the influence of the coating layers of oil left on the cell plates [45], which formed in spite of the extremely low velocity of the front during pistonlike motion. These layers might have effectively reduced the cell gap thickness, and thus increased slightly the distorting pressure in drainage, revealing ultimately the importance of wetting layers in two-phase fluid displacements.

To conclude, an analysis of the local pressure balance at a fluid-fluid front confined in a Hele-Shaw cell explains both qualitatively and quantitatively the sequence of equilibrium configurations reached when the front is driven quasistatically across a localized heterogeneity in the form of a *mesa* defect. This approach accounts for all the features observed experimentally, including metastability, multivaluedness, hysteresis, and pinning in cyclic drainage-imbibition displacements. Its local character makes us think that it may be extended to more realistic disordered media, featuring multiple and randomly distributed constrictions and expansions, thus paving the way to understand the physics behind cooperative fluid displacements (Haines jumps) and their contribution to macroscale pressure-saturation hysteresis in imbibition-drainage cycles.

#### ACKNOWLEDGMENTS

We are grateful to J. F. Joanny, S. Santucci, M. Dentz, and R. Holtzman for fruitful discussions. We also thank X. Clotet for preliminary experiments, and A. Fernández-Nieves and P. Tierno for reading a first draft of the manuscript and providing valuable suggestions and criticisms. R.P. was supported by the Secretary for Universities and Research of the Ministry of Economy and Knowledge of the Government of Catalonia and the COFUND programme of the Marie Curie Actions of the 7th R&D Framework Programme of the European Union (Contract No. 2014 BP-B 00138). This research received financial support from AGAUR (Generalitat de Catalunya) and MINECO (Spain) through Grants No. 2017-SGR-1061 and No. FIS2016-78507-C2-2-P.

- 
- [1] K. Singh, M. Jung, M. Brinkmann, and R. Seemann, Capillary-dominated fluid displacement in porous media, *Annu. Rev. Fluid Mech.* **51**, 429 (2019).
  - [2] M. Sahimi, *Flow and Transport in Porous Media and Fractured Rock* (Wiley VCH Verlag GmbH, New York, 2011).
  - [3] *Multiphase Fluid Flow in Porous and Fractured Reservoirs*, edited by Y.-S. Wu (Gulf Professional Publishing, Boston, 2016).
  - [4] L. Xu, S. Davies, A. B. Schofield, and D. A. Weitz, Dynamics of Drying in 3D Porous Media, *Phys. Rev. Lett.* **101**, 094502 (2008).



- [5] F. Moebius and D. Or, Interfacial jumps and pressure bursts during fluid displacement in interacting irregular capillaries, *J. Colloid Interface Sci.* **377**, 406 (2012).
- [6] S. Berg, H. Ott, S. A. Klapp, A. Schwing, R. Neiteler, N. Brussee, A. Makurat, L. Leu, F. Enzmann, J.-O. Schwarz, M. Kersten, S. Irvine, and M. Stampanoni, Real-time 3D imaging of Haines jumps in porous media flow, *Proc. Natl. Acad. Sci. USA* **110**, 3755 (2013).
- [7] R. T. Armstrong and S. Berg, Interfacial velocities and capillary pressure gradients during Haines jumps, *Phys. Rev. E* **88**, 043010 (2013).
- [8] M. Andrew, B. Bijeljic, and M. J. Blunt, Pore-by-pore capillary pressure measurements using X-ray microtomography at reservoir conditions: Curvature, snap-off, and remobilization of residual CO<sub>2</sub>, *Water Resour. Res.* **50**, 8760 (2014).
- [9] R. T. Armstrong, N. Evseev, D. Koroteev, and S. Berg, Modeling the velocity field during Haines jumps in porous media, *Adv. Water Resour.* **77**, 57 (2015).
- [10] T. Pak, I. B. Butler, S. Geiger, M. I. J. van Dijke, and K. S. Sorbie, Droplet fragmentation: 3D imaging of a previously unidentified pore-scale process during multiphase flow in porous media, *Proc. Natl. Acad. Sci. USA* **112**, 1947 (2015).
- [11] M. Rücker, S. Berg, R. T. Armstrong, A. Georgiadis, H. Ott, A. Schwing, R. Neiteler, N. Brussee, A. Makurat, L. Leu, M. Wolf, F. Khan, F. Enzmann, and M. Kersten, From connected pathway flow to ganglion dynamics, *Geophys. Res. Lett.* **42**, 3888 (2015).
- [12] Y. Edery, S. Berg, and D. Weitz, Surfactant Variations in Porous Media Localize Capillary Instabilities During Haines Jumps, *Phys. Rev. Lett.* **120**, 028005 (2018).
- [13] W. B. Haines, Studies in the physical properties of soil. V. The hysteresis effect in capillary properties, and the modes of moisture distribution associated therewith, *J. Agric. Sci.* **20**, 97 (1930).
- [14] S. Schlüter, S. Berg, M. Rücker, R. T. Armstrong, H. J. Vogel, R. Hilfer, and D. Wildenschild, Pore-scale displacement mechanisms as a source of hysteresis for two-phase flow in porous media, *Water Resour. Res.* **52**, 2194 (2016).
- [15] L. Cueto-Felgueroso and R. Juanes, A discrete-domain description of multiphase flow in porous media: Rugged energy landscapes and the origin of hysteresis, *Geophys. Res. Lett.* **43**, 1615 (2016).
- [16] N. Martys, M. Cieplak, and M.O. Robbins, Critical Phenomena in Fluid Invasion of Porous Media, *Phys. Rev. Lett.* **66**, 1058 (1991).
- [17] F. Moebius and D. Or, Inertial forces affect fluid front displacement dynamics in a pore-throat network model, *Phys. Rev. E* **90**, 023019 (2014).
- [18] J. Xu and M. Y. Louge, Statistical mechanics of unsaturated porous media, *Phys. Rev. E* **92**, 062405 (2015).
- [19] J. E. McClure, R. T. Armstrong, M. A. Berrill, S. Schlüter, S. Berg, W. G. Gray, and C. T. Miller, Geometric state function for two-fluid flow in porous media, *Phys. Rev. Fluids* **3**, 084306 (2018).
- [20] P. G. Saffman and G. I. Taylor, The penetration of a fluid into a porous medium or Hele-Shaw cell containing a more viscous liquid, *Proc. R. Soc. Lond. A* **245**, 312 (1958).
- [21] G. M. Homsy, Viscous fingering in porous media, *Annu. Rev. Fluid Mech.* **19**, 271 (1987).
- [22] R. Lenormand, C. Zarcone, and A. Sarr, Mechanisms of the displacement of one fluid by another in a network of capillary ducts, *J. Fluid Mech.* **135**, 337 (1983).
- [23] M. Cieplak and M.O. Robbins, Dynamical Transition in Quasistatic Fluid Invasion in Porous Media, *Phys. Rev. Lett.* **60**, 2042 (1988).
- [24] M. Cieplak and M. O. Robbins, Influence of contact angle on quasistatic fluid invasion of porous media, *Phys. Rev. B* **41**, 11508 (1990).
- [25] R. Lenormand, Liquids in porous media, *J. Phys.: Condens. Matter* **2**, A79 (1990).
- [26] W. L. Olbricht, Pore-scale prototypes of multiphase flow in porous media, *Annu. Rev. Fluid Mech.* **28**, 187 (1996).
- [27] J. Atencia and D. J. Beebe, Controlled microfluidic interfaces, *Nature (London)* **437**, 648 (2005).
- [28] B. Levaché and D. Bartolo, Revisiting the Saffman-Taylor Experiment: Imbibition Patterns and Liquid-Entrainment Transitions, *Phys. Rev. Lett.* **113**, 044501 (2014).
- [29] B. Zhao, C. W. MacMinn, and R. Juanes, Wettability control on multiphase flow in patterned microfluidics, *Proc. Natl. Acad. Sci. USA* **113**, 10251 (2016).

- [30] C. Odier, B. Levaché, E. Santanach-Carreras, and D. Bartolo, Forced Imbibition in Porous Media: A Fourfold Scenario, *Phys. Rev. Lett.* **119**, 208005 (2017).
- [31] B. Zhao, C. W. MacMinn, B. K. Primkulov, Y. Chen, A. J. Valocchi, J. Zhao, Q. Kang, K. Bruning, J. E. McClure, C. T. Miller *et al.*, Comprehensive comparison of pore-scale models for multiphase flow in porous media, *Proc. Natl. Acad. Sci. USA* **116**, 13799 (2019).
- [32] N. Morrow, Physics and thermodynamics of capillary action in porous media, *Ind. Eng. Chem. Res.* **62**, 32 (1970).
- [33] K. K. Mohanty, H. T. Davis, and L. E. Scriven, Physics of oil entrapment in water-wet rock, *SPE Reservoir Eng.* **2**, 113 (1987).
- [34] K. J. Måløy, L. Furuberg, J. Feder, and T. Jossang, Dynamics of Slow Drainage in Porous Media, *Phys. Rev. Lett.* **68**, 2161 (1992).
- [35] M. Blunt, Pore-level model of wetting, *Phys. Rev. E* **52**, 6387 (1995).
- [36] R. Holtzman and E. Segre, Wettability Stabilizes Fluid Invasion Into Porous Media Via Nonlocal, Cooperative Pore Filling, *Phys. Rev. Lett.* **115**, 164501 (2015).
- [37] R. M. Giordano and J. C. Slattery, Stability of static interfaces in a sinusoidal capillary, *J. Colloid Interface Sci.* **92**, 13 (1983).
- [38] W. W. Liou, Y. Peng, and P. E. Parker, Analytical modeling of capillary flow in tubes of nonuniform cross section, *J. Colloid Interface Sci.* **333**, 389 (2009).
- [39] Y. Méheust, G. Løvoll, K. J. Måløy, and J. Schmittbuhl, Interface scaling in a two-dimensional porous medium under combined viscous, gravity, and capillary effects, *Phys. Rev. E* **66**, 051603 (2002).
- [40] See Supplemental Material at <http://link.aps.org/supplemental/10.1103/PhysRevFluids.5.044002> for (1) the distinction between weak and strong defects, based on the relative strength of distorting and restoring pressures, (2) an effective Landau free energy of the problem, and (3) movies S1 (displacement across a constriction) and S2 (displacement across an expansion)..
- [41] J. F. Joanny and P.-G. de Gennes, A model for contact angle hysteresis, *J. Chem. Phys.* **81**, 552 (1984).
- [42] P.-G. de Gennes, Imperfect Hele-Shaw cells, *J. Phys. (Paris)* **47**, 1541 (1986).
- [43] A. Giacomello, L. Schimmele, and S. Dietrich, Wetting hysteresis induced by nanodefects, *Proc. Natl. Acad. Sci. USA* **113**, E262 (2016).
- [44] A. Paterson, M. Fermigier, P. Jenffer, and L. Limat, Wetting on heterogeneous surfaces: Experiments in an imperfect Hele-Shaw cell, *Phys. Rev. E* **51**, 1291 (1995).
- [45] P. Tabeling, G. Zocchi, and A. Libchaber, An experimental study of the Saffman-Taylor instability, *J. Fluid Mech.* **177**, 67 (1987).
- [46] J. Chopin, A. Prevost, A. Boudaoud, and M. Adda-Bedia, Crack Front Dynamics Across a Single Heterogeneity, *Phys. Rev. Lett.* **107**, 144301 (2011).
- [47] J. Chopin, A. Bhaskar, A. Jog, and L. Ponsou, Depinning Dynamics of Crack Fronts, *Phys. Rev. Lett.* **121**, 235501 (2018).
- [48] F. Moebius, D. Canone, and D. Or, Characteristics of acoustic emissions induced by fluid front displacement in porous media, *Water Resour. Res.* **48**, 1 (2012).